

Article

P-Stereogenic Phosphines for the Stabilisation of Metal Nanoparticles. A Surface State Study

Eva Raluy¹, Arnald Grabulosa², Pierre Lavedan³, Christian Pradel¹, Guillermo Muller², Isabelle Favier^{1,*} and Montserrat Gómez^{1,*}

¹ Université de Toulouse 3—Paul Sabatier, Laboratoire Hétérochimie Fondamentale et Appliquée (LHFA), 118 Route de Narbonne, 31062 Toulouse CEDEX 9, France and CNRS, LHFA UMR 5069, 31062 Toulouse CEDEX 9, France; eraluy@iciq.es (E.R.); radel@chimie.ups-tlse.fr (C.P.)

² Departament de Química Inorgànica i Orgànica, Secció de Química Inorgànica, Universitat de Barcelona, Martí i Franquès 1-11, 08028 Barcelona, Spain; arnald.grabulosa@qi.ub.es (A.G.); guillermo.muller@qi.ub.es (G.M.)

³ Service Commun RMN, ICT, Université de Toulouse, UPS, 118 Route de Narbonne, 31062 Toulouse CEDEX 9, France; lavedan@chimie.ups-tlse.fr

* Correspondence: favier@chimie.ups-tlse.fr (I.F.); gomez@chimie.ups-tlse.fr (M.G.); Tel.: +33-5-61-55-62-87 (I.F.); 33-5-61-55-77-38 (M.G.)

Academic Editors: Alain Roucoux and Audrey Denicourt

Received: 9 November 2016; Accepted: 13 December 2016; Published: 20 December 2016

Abstract: Palladium and ruthenium nanoparticles have been prepared following the organometallic precursor decomposition methodology, under dihydrogen pressure and in the presence of borane protected *P*-stereogenic phosphines. NMR (Nuclear Magnetic Resonance) monitoring of the corresponding syntheses has permitted to determine the optimal metal/ligand ratio for leading to small and well-dispersed nanoparticles. Exchange ligand reactions of the as-prepared materials have proven the strong interaction of the phosphines with the metal surface; only oxidative treatment using hydrogen peroxide could release the phosphine-based stabiliser from the metal surface. Pd and Ru nanoparticles have been evaluated in hydrogenation reactions, confirming the robustness of the stabilisers, which selectively permitted the hydrogenation of exocyclic C=C bonds, preventing the coordination of the aromatic rings and as a result, their hydrogenation.

Keywords: *P*-stereogenic phosphines; metal nanoparticles; palladium; ruthenium; surface reactivity

1. Introduction

Even if more and more organic transformations are using metal nanoparticles (MNPs) as catalysts [1–6], few of them concern enantioselective processes (for selected reviews, see [7–10]). The enantioselective catalysis on surfaces is commonly explained by three main mechanisms: the presence of chiral crystalline atomic structures at the surface, chiral adsorbates which modify the surface and chiral modifiers which control the approach of the substrate on the surface [11,12]. The stereoselective reactions mainly concern hydrogenations and C-C bond formation reactions based on the third mechanism [13–31]. In this context, the optically pure ligand should be able to generate both a strong enough coordination at the metallic surface to stabilize MNPs and an asymmetric environment to efficiently lead to one of the expected stereoisomers during the organic transformation. Ligands coordinate at the metallic surface by different ways, such as dative donor bonds between heteroatoms of the ligands and the metal surface, and also by π -interactions through aromatic fragments of the ligands and the nanoparticle. The nature of the chiral stabilisers reported in the synthesis of MNPs is wide-ranging, including dienes [15], cinchona alkaloids [16–18], mono or bidentate amines [19–21], phosphorus-based ligands (phosphites [22–26], diphosphines [27–30], secondary phosphine oxide [31]). *P*-stereogenic phosphines are well-known in

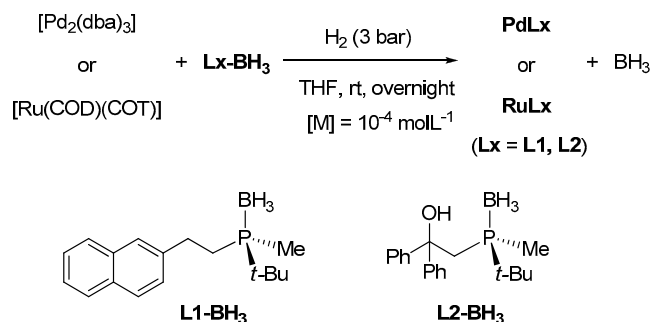
homogeneous catalysis using organometallic complexes as catalytic precursors, finding applications in hydrogenation, transfer hydrogenation, cyclopropanation, hydrovinylation, Diels Alder reactions and allylic substitutions [32–34]. However and to the best of our knowledge, no *P*-stereogenic phosphanes have been previously used as stabilisers of MNPs-based catalysts.

Herein we describe the synthesis of ruthenium and palladium nanoparticles stabilised by *P*-stereogenic phosphines and their coordination to the metallic surface. A study of hydrogenation of C=C bonds was carried out with the purpose to understand the interaction of these stabilisers with the metal surface.

2. Results and Discussion

2.1. Synthesis and Characterisation of PdNPs and RuNPs

We prepared palladium (**PdLx**) and ruthenium (**RuLx**) nanoparticles (**Lx** = **L1** or **L2**, Scheme 1), containing optically pure borane-protected phosphines, (*S*)-*tert*-butylmethyl(2-(2-naphthyl)ethyl) phosphine-borane (**L1-BH₃**) [35] and (*R*)-(2,2-diphenyl-2-hydroxyethyl)-*P*-methyl-*tert*-butyl-phosphine-borane (**L2-BH₃**) [36], as stabilisers. Based on the literature [37–39], MNPs were synthesised by organometallic complex decomposition in the presence of the corresponding ligand (**L1** or **L2**) using a metal/ligand ratio of 1/0.2, under hydrogen atmosphere (3 bar); [Pd₂(dba)₃] (dba = dibenzylideneacetone) and [Ru(COD)(COT)] (COD = 1,5-cyclooctadiene; COT = 1,3,5-cyclooctatriene) were chosen as organometallic precursors (Scheme 1).



Scheme 1. Synthesis of PdNPs (**PdL1**, **PdL2**) and RuNPs (**RuL1**, **RuL2**) by organometallic precursor decomposition methodology.

The as-prepared materials were analysed by TEM, evidencing the formation of small and well-dispersed ruthenium nanoparticles, **RuL1** and **RuL2** (mean size, ca. 1.2 nm; Figure 1). In contrast, PdNPs led to more agglomerated systems (Figure 1). Infrared spectra of these materials revealed the absence of borane, meaning that BH₃, protecting group of the phosphines, was removed during the synthesis of the corresponding MNPs (see Figure S1 in the Supplementary Materials).

With the aim of determining the optimal metal/ligand ratio to give well-dispersed nanoparticles, a multi-nuclear NMR monitoring study of the synthesis of these MNPs was carried out. For this purpose, a mixture of the corresponding organometallic complex and the corresponding ligand in 1 mL of THF-*d*₈ was prepared and pressurised with dihydrogen (3 bar; NMR tube with PTFE (polytetrafluoroethylene) Young valve), in the presence of dodecane as internal standard. With the purpose to quantify the amount of capped ligand at the MNP surface, an excess of ligand was used (a metal/L ratio of 1/1). The intensity decrease of the *t*-Bu doublet signal (1.2 ppm; ³J_{H-P} = 12 Hz) in the corresponding ¹H NMR spectra, was used as probe to determine the percentage of ligand adsorbed at the metallic surface (see Figures S2–S5 in the Supplementary Materials). The mixtures were monitored until unchanged ¹H NMR spectra were recorded. For PdNPs, 0.4 equivalent of free ligand remained in the solution for both **PdL1** and **PdL2**, meaning that the Pd/L ratio in the formed PdNPs was 1/0.6 (Figure 2). TEM (Transmission Electron Microscopy) analyses after the NMR monitoring showed the

exclusive formation of nanoparticles of size 1.4 nm for both ligands (Figure 2), in contrast with the agglomerates obtained using a Pd/L ratio of 1/0.2 (Figure 1).

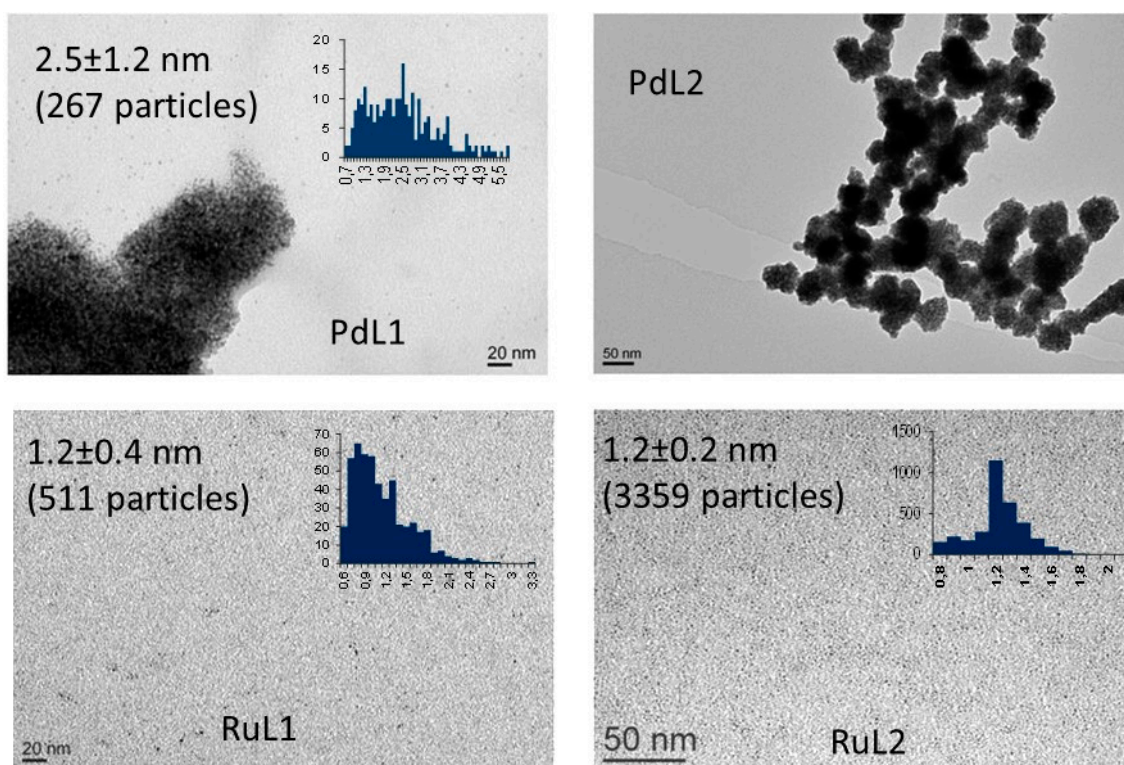


Figure 1. TEM (Transmission Electron Microscopy) images of PdL1 and PdL2 (top); and RuL1 and RuL2 (bottom); insets represent the corresponding size distribution diagrams.

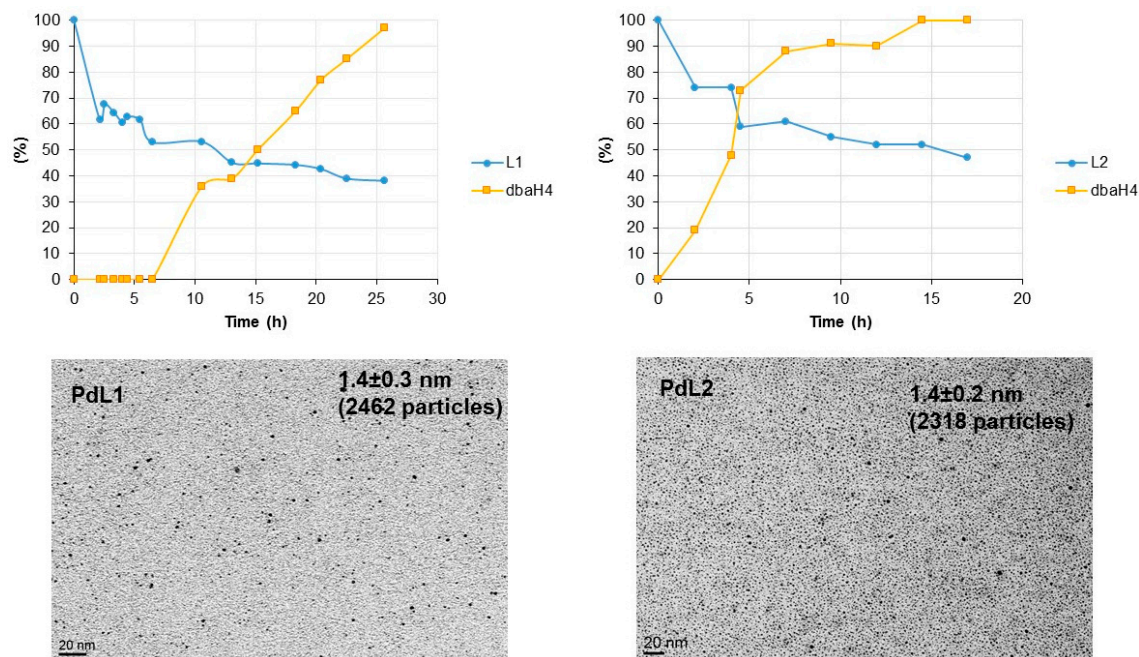


Figure 2. Graphical representations of the data corresponding to the consumption of ligand and decomposition of Pd precursor from the ^1H NMR monitoring of the formation PdNPs with L1 and L2 (top); TEM images of PdL1 and PdL2 after total consumption of $[\text{Pd}_2(\text{dba})_3]$ (bottom).

In the case of ruthenium, only 0.4 equivalent of ligand was necessary for the formation of RuNPs, **RuL1** and **RuL2** (Figure 3). Contrary to the behaviour of the formation of PdNPs, the decomposition of [Ru(COD)(COT)] was slower (the NMR tube was regularly shaken in order to observe evolution of the decomposition of the organometallic precursor). TEM analyses of the particles after the NMR monitoring exhibited nanoparticles of size 1.2 nm for both ligands (Figure 3), analogously to those obtained using a Ru/L ratio of 1/0.2 (Figure 1).

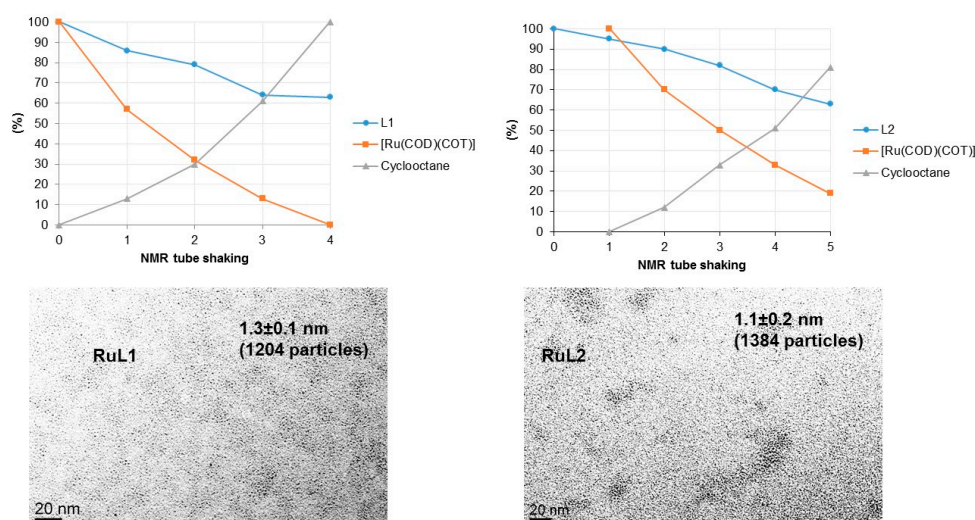


Figure 3. Graphical representations of the data corresponding to the consumption of ligand and [Ru(COD)(COT)], and formation of cyclooctane (top); TEM images of **RuL1** and **RuL2** after total consumption of [Ru(COD)(COT)] (bottom).

The decomposition of the metallic precursors, [Pd₂(dba)₃] and [Ru(COD)(COT)], was also checked by the concomitant formation of dbaH₄ (dbaH₄ = 1,5-diphenylpenta-3-one) and cyclooctane, respectively.

The formation of PdNPs was also monitored by the intensity decrease of the corresponding ³¹P and ¹¹B NMR signals, in addition to the disappearance of the ¹H NMR ligand signals (see Figure S6 in the Supplementary Materials); other signals corresponding to molecular palladium species could be also observed, together with the formation of free BH₄[−], which indicates that the ligand adsorbed on the surface corresponds to the BH₃-free phosphine. In the case of the formation of RuNPs, the differences in intensity of ³¹P and ¹¹B NMR signals were less perceptible (see Figure S7 in the Supplementary Materials).

With this information, PdNPs and RuNPs were synthesised at a larger scale, using now a metal/ligand ratio of 1/0.6 and 1/0.4, respectively, preserving the conditions previously described (see above, Scheme 1). Under these conditions, PdNPs with a mean diameter of ca. 1.5 nm for both ligands were obtained (Figure 4). Electronic diffraction analyses of these PdNPs showed a fcc structure as expected for bulk Pd(0) and the corresponding EDX (Energy dispersive X-ray spectroscopy) data evidenced the presence of ligand in the as-prepared nanoparticles (see Figure S8 in the Supplementary Materials). Elemental analyses indicated that the Pd/L ratio found on the isolated PdNPs was: **Pd/L1** = 1/0.27 and **Pd/L2** = 1/0.50 (corresponding to a ratio Pd/L at the surface **PdL1_{0,4}** and **PdL2_{0,8}**). Concerning RuNPs, small nanoparticles were also obtained, with a mean diameter of 1.0 and 1.2 nm for **RuL1** and **RuL2**, respectively. Their electronic diffraction analyses exhibited a hcp arrangement characteristic of bulk Ru(0); the corresponding EDX data confirmed the presence of the ligand in the as-prepared materials. Elemental analyses indicated that the Ru/L ratio found on the isolated RuNPs was: **Ru/L1** = 1/0.56 and **Ru/L2** = 1/0.46 (corresponding to a ratio Pd/L at the surface **PdL1_{0,4}** and **PdL2_{0,8}**).

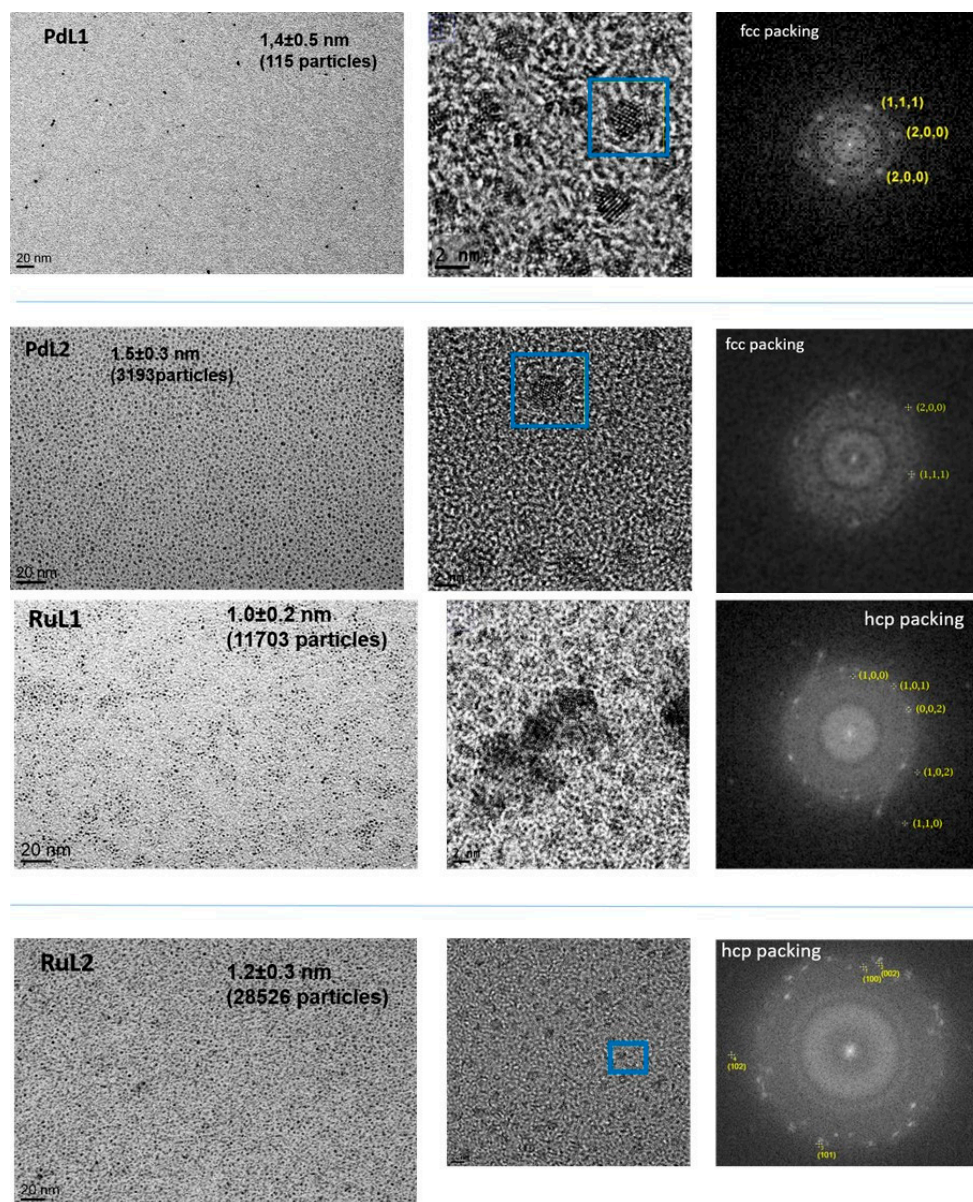


Figure 4. TEM (left), HR-TEM (middle) and electronic diffraction (right) images of PdNPs and RuNPs stabilised by L1 and L2.

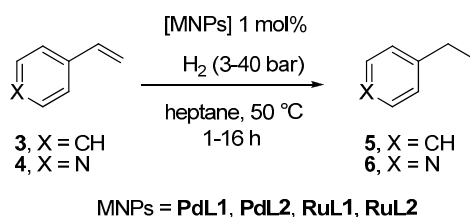
The synthesis of MNPs was also run with borane-free L2 with both metal precursors, $[\text{Pd}_2(\text{dba})_3]$ and $[\text{Ru}(\text{COD})(\text{COT})]$ (under the same conditions than those described above using a metal/ligand ratio of 1/0.6 and 1/0.4 for Pd and Ru, respectively). Small MNPs of the approximately 1.0 nm were obtained for both metals (see Figure S9 in the Supplementary Materials).

In a previous work, we could prove that ligands can be modified during the synthesis of metal nanoparticles [40]. In order to recover the stabiliser after synthesis of the corresponding MNPs, ligand exchange reactions were carried out [41]. Therefore, taking advantage of the affinity of noble-based metal surfaces by thiols and carbon monoxide, dodecanethiol and CO (up to 3 bar of pressure) were added to the solution of MNPs dispersed in THF- d_8 , with the aim of releasing the corresponding phosphine from the metallic surface. In any case, ligand exchange occurred (monitored by ^1H and ^{31}P NMR during one week at room temperature). Only oxidative conditions allowed the observation of free stabilisers. Therefore, treatment of PdNPs with hydrogen peroxide showed the presence of the corresponding oxides of L1 and L2, by both ^{31}P NMR and mass spectrometry (see Figures S10 and S11

in the Supplementary Materials). This behaviour evidenced that both ligands interact strongly with the palladium surface. The same oxidative treatment was applied to preform RuNPs, but unfortunately the detection of the corresponding oxides was not possible.

2.2. Hydrogenation Reactivity

As benchmark reactions, we chose to study the catalytic behaviour of the prepared PdNPs and RuNPs in the hydrogenation of both styrene (**3**) and 4-vinylpyridine (**4**), because of the different functions to be hydrogenated (arene and vinyl moieties) and the different ability to coordinate to the metal surface (phenyl versus pyridyl group) (Scheme 2 and Table S1 Supplementary Materials) [42]. For both substrates using any of the Ru- or Pd-based catalysts, we observed the exclusive formation of ethylbenzene (**5**) and 4-ethylpyridine (**6**), under relative smooth conditions, 3 bar H₂ pressure at 50 °C (Scheme 2). PdNPs were more active than RuNPs, achieving full conversion after 1 h and 16 h, respectively. With the aim of triggering the reduction of the aromatic group, hydrogenations at higher pressures (up to 40 bar) using RuNPs as catalysts were carried out. However no arene-hydrogenation was favoured; only under 40 bar H₂, we could observe the presence of traces of ethylcyclohexane and 4-ethylpiperidine (ca. 5%), in addition to the corresponding ethyl derivatives **5** and **6**. A similar catalytic trend has been reported for achiral phosphines [43]. Unfortunately, RuNPs were not active in the hydrogenation of the carbonyl group of acetophenone (under 40 bar H₂ at 50 °C overnight).



Scheme 2. Hydrogenation of styrene (**3**) and 4-vinylpyridine (**4**) catalysed by Pd- and Ru-based catalysts.

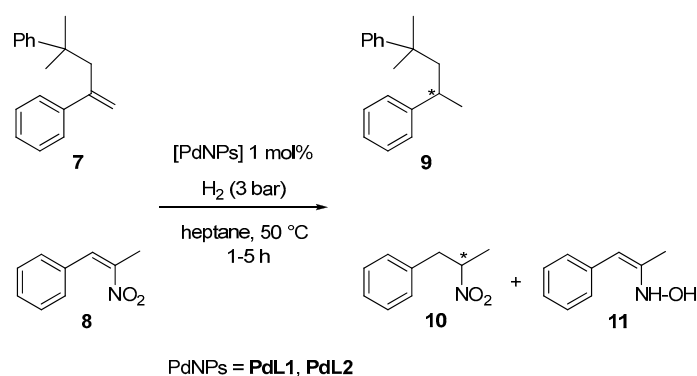
These results certainly evidence that both phosphines remain robustly linked to the surface (as proven by the ligand exchange reactions performed; see above), hindering the approach of the aromatic group of the substrates **3** or **4** at the metal surface; only the vinyl group is consequently able to be reduced. Furthermore, this assumption is supported by the fact that [Ru(COD(COT))] used as catalytic precursor in the absence of any ligand, gave, under 20 bar H₂ for 16h of reaction, a mixture of ethylbenzene and ethylcyclohexane (64% and 36%, respectively). The behaviour observed using **RuL1** and **RuL2** contrasts with that described for RuNPs stabilised by phosphines, for which the reduction of the aromatic fragments occurs [28,44–48]. In our case, **L1** and **L2** can be coordinated to the metal surface in a bidentate mode by the dative M-P bond and a secondary interaction: π interaction by the naphthyl group (**L1**) or interaction by the alcohol function or phenyl group (**L2**), decreasing the vacant coordination sites on nanoparticles. This coordination mode means that the compact faces on nanoparticles are occupied, avoiding the coordination of arene substrates [49].

Therefore, the lack of hydride transfer from the metal surface to the aromatic cycles is most likely due to a high coverage of the surface by the phosphines (**L1**, **L2**). Thus, these saturated surfaces favour the chemisorption of C=C vinyl bond (adsorption enthalpy, ca. -20 kJ/mol) in relation to the chemisorption of an aromatic cycle (adsorption enthalpy, ca. -70 kJ/mol) [50]. This presumption is in agreement with the non-coordinated mechanism proposed by Sautet and co-workers for the hydrogenation of exocyclic C=C bonds [49].

We also analysed by ICP-AES the product **6** obtained by hydrogenation of 4-vinylpyridine (**4**) using both **PdL2** and **RuL2**; the metal content was lower than 1 ppm (for Ru: 0.7 ppm; for Pd: 0.08 ppm), what indicates an irrelevant metal leaching. With the aim of elucidating the catalyst nature, we added mercury to the hydrogenation of **4** using both **PdL2** and **RuL2** after 5 min of reaction at room temperature under 1 bar H₂ pressure (conversion: 16% for **PdL2**; 5% for **RuL2**); the reaction was

then heated at 50 °C under 3 bar overnight, obtaining full conversion of 4-vinylpyridine in both cases. These results point to a homogeneous catalytic behaviour, in contrast with the ICP analyses of the hydrogenated products. This behaviour seems to evidence that preformed MNPs act as a reservoir of homogeneous active species, being again aggregated at the end of the reaction in agreement with the insignificant content of metal on the isolated products.

Taking into account that **L1** and **L2** are optically pure, we decided to test the hydrogenation of prochiral substrates, in particular styrene derivatives (**7**, **8**) using Pd-based catalysts (Scheme 3). For substrate **7**, the same behaviour than that observed for styrene was observed: full conversion towards **9** after 1 h of reaction. However the hydrogenation of **8** was less efficient (only 25% conversion after 5 h of reaction), probably due to its higher steric-demanding effect, and led to a mixture of **10** and the hydroxylamine **11** (the oxime tautomer was not observed by ¹H NMR). Unfortunately no asymmetric induction was observed in any case; this absence of enantioselectivity cannot be attributed to the racemization of the chiral ligands, as proven by the control experiment using **L1** as substrate under catalytic conditions [see experimental section].



Scheme 3. Hydrogenation of prochiral substrates catalysed by PdL1 and PdL2 catalysts.

3. Materials and Methods

3.1. General

Unless otherwise stated, all chemical reagents were obtained from commercial suppliers and used without further purification. Optically pure borane-protected phosphines, (*S*)-*tert*-butylmethyl (2-(2-naphthyl)ethyl)phosphine-borane (**L1-BH₃**) and (*R*)-(2,2-diphenyl-2-hydroxyethyl)-*P*-methyl-*t*-butyl-phosphine-borane (**L2-BH₃**) were synthesised as previously described [35,36]. All manipulations were performed using standard Schlenk techniques under argon atmosphere. NMR spectra were recorded on a Bruker Avance 400 spectrometer (Bruker, Billerica, MA, USA) at 293 K (400 MHz for ¹H NMR; 162 MHz for ³¹P NMR; 128 MHz for ¹¹B NMR). GC analyses were carried out on a GC Perkin Elmer Clarus 500 with ionization flame detector (Waters, Waltham, MA, USA), using a SGE BPX5 column composed by 5% phenylmethylsiloxane and a Perkin Elmer Clarus MS560 mass detector. The determination of enantiomeric excesses was carried out on a UPLC Acquity Waters at 40 °C with a UV PDA detector (Waters, Milford, Massachusetts, United States) and a cyclobond I2000HP RSP15cm/4.6 5 μm column with a mixture of H₂O/CH₃CN = 60/40. TEM images of particles in the solid state and dispersed in glycerol were obtained from transmission electron microscopes JEOL JEM (JEOLn Akishima, Tokyo, Japan) 1400 running at 120 kV and HR-TEM from JEOL JEM 2100F running at 200 kV equipped with X PGT (detection of light elements, resolution 135 eV). The nanoparticles size, distribution and average diameter were determined from TEM images with Image-J software (Image processing, Public domain, <https://imagej.nih.gov/ij/>) associated to a Microsoft Excel macro developed by Christian Pradel. IR spectra were recorded in the range of 4000–400 cm⁻¹ on a Varian 640-IR FTIR Spectrometer (Varian, Salt Lake City, United States). High-pressure reactions were carried

out in a Top Industrie Autoclave suitable from 0 to 50 bar and from 15 to 150 °C (Top Industrie, Vaux Le Pénil, France). Elemental and ICP-AES analyses were carried out at the “Service d’Analyse” of Laboratoire de Chimie de Coordination (Toulouse) using a Perkin Elmer 2400 series II analyser (Perkin Elmer, Waltham, MA, USA) and by Antellis respectively.

3.2. Synthesis of PdNPs and RuNPs Stabilised by Optically Pure Borane-Protected Phosphines, **L1-BH₃** and **L2-BH₃**

As a standard procedure, the organometallic complex (37 mg of [Pd₂(dba)₃] (0.04 mmol) or 25 mg [Ru(COD)(COT)] (0.08 mmol)) was dissolved in a solution of 80 mL of THF with 0.6 eq. of **L-BH₃** (14 mg of **L1-BH₃** or 15 mg for **L2-BH₃**) in a Fischer–Porter bottle. The mixture was then pressurised under dihydrogen (3 bar) at room temperature. The vigorous stirring and dihydrogen pressure were maintained for 18h at room temperature, leading to black and homogeneous colloidal solutions. The solvent was then evaporated. The particles as black solids were washed with pentane (3 × 10 mL) and dried under vacuum. The nanoparticles were characterised by TEM, IR and elemental analysis.

PdL1_{0.4} TEM: mean size 1.4 nm; elemental analysis: % found: 61.3% Pd, 28.70% C, 3.22% H; % calculated for Pd₁(C₁₇H₂₆P₁B₁)_{0.27} 60.9% Pd, 31.66% C, 4.06% H

PdL2_{0.8} TEM: mean size 1.9 nm; elemental analysis: % found: 40.9% Pd, 43.0% C, 4.39% H; % calculated for Pd₁(C₁₉H₂₈O₁P₁B₁)_{0.50} 40.77% Pd, 42.97% C, 5.28% H

RuL1_{0.7} TEM: mean size 1.0 nm; elemental analysis: % found: 31.0% Ru, 34.66% C, 5.08% H; % calculated for Ru₁(C₁₇H₂₆P₁B₁)_{0.56} + 4.7 H₂O 30.89% Ru, 34.94% C, 7.33% H

RuL2_{0.6} TEM: mean size 1.2 nm; elemental analysis: % found: 36.9% Ru, 38.42% C, 4.88% H; % calculated for Ru₁(C₁₉H₂₈O₁P₁B₁)_{0.46} + 1.6 H₂O 36.86% Ru, 38.28% C, 4.53% H.

3.3. Hydrogenation Reactions Catalysed by PdNPs and RuNPs

2 mg of RuNPs (0.01 mmol Ru) or 3 mg of PdNPs (0.01 mmol Pd) and the corresponding substrate (1 mmol of **3** (105 mg), **4** (104 mg), **7** (236 mg) or **8** (163 mg)) were dissolved in 20 mL heptane at room temperature, in the presence of 142 mg of decane as internal standard. The catalytic mixture was stirred, pressurized under the desired pressure (3–40 bar) and heated at 50 °C overnight in an autoclave or in a Fisher-Porter bottle. The system was then depressurized, the solution was filtered on celite and analyzed by GC.

3.4. Hydrogenation of **L1**

3 mg of PdNPs (0.01 mmol Pd) and **L1-BH₃** (15 mg, 0.055 mmol) were dissolved in 10 mL heptane at room temperature. The catalytic mixture was stirred, pressurized under 3 bar and heated at 50 °C overnight in Fisher-Porter bottle. The system was then depressurized, the solution was filtered on celite and analyzed by ¹H, ¹¹B and ³¹P NMR. [α]²³_D (c = 10 mg·mL⁻¹, CHCl₃) = −11.3° (for pure ligand, [α]²³_D (c = 10 mg·mL⁻¹, CHCl₃) = −10.7° [30]).

4. Conclusions

In summary, *P*-stereogenic phosphines **L1** and **L2** have proven their efficiency to stabilise small and well-dispersed palladium and ruthenium nanoparticles, depending on the metal/ligand ratio used. The NMR monitoring of the syntheses of MNPs together with the TEM analyses of the resulting colloidal solutions, allowed us knowing the appropriate amount of ligand-to-metal in order to get non agglomerated materials. The coordination strength of the stabilisers at the metal surface is crucial to understand their aptitude as catalysts. With this purpose in mind, we studied exchange ligand reactions between the as-prepared nanoparticles and ligands such as thiols and carbon monoxide, demonstrating that **L1** and **L2** are robust, and only oxidative treatments (reaction of MNPs with hydrogen peroxide) permitted to de-coordinate the phosphines from the surface. This ligand robustness can be explained by a bidentate coordination mode, through both the phosphorus centre and the aryl or alcohol functions present in the phosphine structure. This behaviour could be also reflected in the hydrogenation

of vinyl-aromatic substrates catalysed by the MNPs. In particular, Ru-based catalysts exclusively hydrogenated the corresponding vinyl groups, because the aromatic rings of the substrates cannot come close to the metal surface, due to the coverage of the faces of nanoparticles by the phosphines. Unfortunately, no enantioselectivity could be induced.

Supplementary Materials: The following are available online at www.mdpi.com/2073-4344/6/12/213/s1, Synthesis of PdNPs and RuNPs, hydrogenation reactions Figure S1: IR spectra (KBr pellets) of ligands **L1** and **L2** and the corresponding MNPs: **PdL1**, **PdL2**, **RuL1** and **RuL2**, Figure S2: ^1H NMR (400 MHz, solvent, 298 K) spectra corresponding to the monitoring of the formation of **PdL1**, Figure S3: ^1H NMR (400 MHz, solvent, 298 K) spectra corresponding to the monitoring of the formation of **PdL2**, Figure S4: ^1H NMR (400 MHz, solvent, 298 K) spectra corresponding to the monitoring of the formation of **RuL1**, Figure S5: ^1H NMR (400 MHz, solvent, 298 K) spectra corresponding to the monitoring of the formation of **PdL2**, Figure S6: ^{31}P (162 MHz, solvent, 298 K) and ^{11}B (128 MHz, solvent, 298 K) NMR monitoring of the formation of **PdL1** (top) and **PdL2** (bottom), Figure S7: ^{31}P (162 MHz, solvent, 298 K) and ^{11}B (128 MHz, solvent, 298 K) NMR monitoring of the formation of **RuL1** and **RuL2**, Figure S8: EDX (Energy Dispersive X-ray) analyses of **PdL1**, **RuL1** and **RuL2**, Figure S9: TEM images of **PdL2** and **RuL2** NPs stabilised with borane-free phosphine ligand, with the corresponding size distribution diagrams, Figure S10: Mass spectrometry analyses of an organic phase of **PdL1** treated with $\text{H}_2\text{O}_2(\text{aq})$ and extracted with CH_2Cl_2 (FAB and DCI/ NH_3 analyses), Figure S11: Mass spectrometry analyses of an organic phase of **PdL2** treated with $\text{H}_2\text{O}_2(\text{aq})$ and extracted with CH_2Cl_2 (FAB and DCI/ NH_3 analyses), Figure S12: ^{31}P NMR spectra in CDCl_3 of PdNPs before and after addition of $\text{H}_2\text{O}_2(\text{aq})$, Table S1. Hydrogenation of styrene and 4-vinylpyridine catalysed by **PdL** and **RuL** (**L** = **L1**, **L2**).

Acknowledgments: Financial support from the Centre National de la Recherche Scientifique (CNRS), the Université de Toulouse 3—Paul Sabatier and Ministerio de Economía y Competitividad (grant number CTQ2015-65040-P) is gratefully acknowledged.

Author Contributions: E.R. carried out the synthesis of MNPs; A.G. carried out the synthesis of phosphines; P.L. performed NMR monitoring analyses; C.P. performed (HR) TEM and EDX analyses; G.M., I.F. and M.G. conceived the work and wrote the manuscript.

Conflicts of Interest: The authors declare no conflict of interest.

References

1. Bönemann, H.; Richards, R.M. Nanoscopic Metal Particles—Synthetic Methods and Potential Applications. *Eur. J. Inorg. Chem.* **2001**, *2001*, 2455–2480. [[CrossRef](#)]
2. Reetz, M.T.; Helbig, W.; Quaiser, S.A.; Stimming, U.; Breuer, N.; Vogel, R. Visualization of Surfactants on Nanostructured Clusters by a Combination of STM and High-Resolution TEM. *Science* **1995**, *267*, 367–369. [[CrossRef](#)] [[PubMed](#)]
3. Trapp, O.; Weber, S.K.; Bauch, S.; Hofstadt, W. High-Throughput Screening of Catalysts by Combining Reaction and Analysis. *Angew. Chem. Int. Ed.* **2007**, *46*, 7307–7310. [[CrossRef](#)] [[PubMed](#)]
4. Trapp, O.; Weber, S.K.; Bauch, S.; Bäcker, T.; Hofstadt, W.; Spliethoff, B. High Throughput Kinetic Study of Hydrogenations over Palladium Nanoparticles—Combination of Reaction and Analysis. *Chem. Eur. J.* **2008**, *14*, 4657–4666. [[CrossRef](#)] [[PubMed](#)]
5. Gmeiner, J.; Seibicke, M.; Behrens, S.; Spliethoff, B.; Trapp, O. Investigation of the Hydrogenation of 5-Methylfurfural by Noble Metal Nanoparticles in a Microcapillary Reactor. *ChemSusChem* **2016**, *6*, 583–587. [[CrossRef](#)] [[PubMed](#)]
6. Gmeiner, J.; Behrens, S.; Spliethoff, B.; Trapp, O. Ruthenium Nanoparticles in High-Throughput Studies of Chemoselective Carbonyl Hydrogenation Reactions. *ChemCatChem* **2016**, *8*, 571–576. [[CrossRef](#)]
7. Yasukawa, T.; Miyamura, H.; Kobayashi, S. Chiral metal nanoparticle-catalyzed asymmetric C–C bond formation reactions. *Chem. Soc. Rev.* **2014**, *43*, 1450–1461. [[CrossRef](#)] [[PubMed](#)]
8. Barbaro, P.; Dal Santo, V.; Liguori, F. Emerging strategies in sustainable fine-chemical synthesis: Asymmetric catalysis by metal nanoparticles. *Dalton Trans.* **2010**, *39*, 8391–8402. [[CrossRef](#)] [[PubMed](#)]
9. Roy, S.; Pericàs, M.A. Functionalized nanoparticles as catalysts for enantioselective processes. *Org. Biomol. Chem.* **2009**, *7*, 2669–2677. [[CrossRef](#)] [[PubMed](#)]
10. Favier, I.; Madec, D.; Teuma, E.; Gómez, M. Palladium nanoparticles applied in organic synthesis as catalytic precursors. *Curr. Org. Chem.* **2011**, *15*, 3127–3174. [[CrossRef](#)]
11. Gellman, A.J.; Tysoe, W.T.; Zaera, F. Surface Chemistry for Enantioselective Catalysis. *Catal. Lett.* **2015**, *145*, 220–232. [[CrossRef](#)]

12. Mallat, T.; Orglmeister, E.; Baiker, A. Asymmetric Catalysis at Chiral Metal Surfaces. *Chem. Rev.* **2007**, *107*, 4863–4890. [[CrossRef](#)] [[PubMed](#)]
13. Gual, A.; Godard, C.; Castellón, S.; Claver, C. Soluble transition-metal nanoparticles-catalysed hydrogenation of arenes. *Dalton Trans.* **2010**, *39*, 11499–11512. [[CrossRef](#)] [[PubMed](#)]
14. Studer, M.; Blaser, H.-U.; Exner, C. Enantioselective Hydrogenation Using Heterogeneous Modified Catalysts: An Update. *Adv. Synth. Catal.* **2003**, *345*, 45–65. [[CrossRef](#)]
15. Yasukawa, T.; Suzuki, A.; Miyamura, H.; Nishino, K.; Kobayashi, S. Chiral Metal Nanoparticle Systems as Heterogeneous Catalysts beyond Homogeneous Metal Complex Catalysts for Asymmetric Addition of Arylboronic Acids to α,β -Unsaturated Carbonyl Compounds. *J. Am. Chem. Soc.* **2015**, *137*, 6616–6623. [[CrossRef](#)] [[PubMed](#)]
16. Hong, J.; Lee, I.; Zaera, F. Correlated bifunctionality in heterogeneous catalysts: Selective tethering of cinchonidine next to supported Pt nanoparticles. *Catal. Sci. Technol.* **2015**, *5*, 680–689. [[CrossRef](#)]
17. Kirby, F.; Moreno-Marrodan, C.; Baán, Z.; Bleeker, B.F.; Barbaro, P.; Berben, P.H.; Witte, P.T. NanoSelect Precious Metal Catalysts and their Use in Asymmetric Heterogeneous Catalysis. *ChemCatChem* **2014**, *6*, 2904–2909. [[CrossRef](#)]
18. Schmidt, E.; Vargas, A.; Mallat, T.; Baiker, A. Shape-Selective Enantioselective Hydrogenation on Pt Nanoparticles. *J. Am. Chem. Soc.* **2009**, *131*, 12358–12367. [[CrossRef](#)] [[PubMed](#)]
19. Gross, E.; Dean Toste, F.; Somorjai, G.A. Polymer-Encapsulated Metallic Nanoparticles as a Bridge between Homogeneous and Heterogeneous Catalysis. *Catal. Lett.* **2015**, *145*, 126–138. [[CrossRef](#)]
20. Lili, L.; Xin, Z.; Shumin, R.; Ying, Y.; Xiaoping, D.; Jinsen, G.; Chunming, X.; Jing, H. Catalysis by metal–organic frameworks: Proline and gold functionalized MOFs for the aldol and three-component coupling reactions. *RSC Adv.* **2014**, *4*, 13093–13107. [[CrossRef](#)]
21. Khair, N.; Navas, N.; Elhalem, E.; Valdivia, V.; Fernandez, I. Proline-coated gold nanoparticles as a highly efficient nanocatalyst for the enantioselective direct aldol reaction in water. *RSC Adv.* **2013**, *3*, 3861–3864. [[CrossRef](#)]
22. Jansat, S.; Gómez, M.; Philippot, K.; Muller, G.; Guiu, E.; Claver, C.; Castellón, S.; Chaudret, B. A Case for Enantioselective Allylic Alkylation Catalyzed by Palladium Nanoparticles. *J. Am. Chem. Soc.* **2004**, *126*, 1592–1593. [[CrossRef](#)] [[PubMed](#)]
23. Favier, I.; Balanta Castillo, A.; Godard, C.; Castellón, S.; Claver, C.; Gómez, M.; Teuma, E. Efficient recycling of a chiral palladium catalytic system for asymmetric allylic substitutions in ionic liquid. *Chem. Commun.* **2011**, *47*, 7869–7871. [[CrossRef](#)] [[PubMed](#)]
24. Dieguez, M.; Pamies, O.; Mata, Y.; Teuma, E.; Gómez, M.; Ribaudó, F.; van Leeuwen, P.W.N.M. Palladium nanoparticles in allylic alkylations and Heck reactions: The molecular nature of the catalyst studied in a membrane reactor. *Adv. Synth. Catal.* **2008**, *350*, 2583–2598. [[CrossRef](#)]
25. Gual, A.; Axet, M.R.; Philippot, K.; Chaudret, B.; Denicourt-Nowicki, A.; Roucoux, A.; Castellón, S.; Claver, C. Diphosphite ligands derived from carbohydrates as stabilizers for ruthenium nanoparticles: Promising catalytic systems in arene hydrogenation. *Chem. Commun.* **2008**, 2759–2761. [[CrossRef](#)] [[PubMed](#)]
26. Mella, C.; Ávila, M.; Sánchez, A.; Marzioletti, T.; Reyes, P.; Ruiz, D. Chiral Rh/SiO₂ catalysts for enantioselective hydrogenation reactions. The role of (*S,S*)-DIPAMP as chiral modifier and stabilizer on metallic nanoparticles synthesis. *J. Chil. Chem. Soc.* **2013**, *58*, 2125–2130. [[CrossRef](#)]
27. Ruiz, D.; Mella, C.; Fierro, J.L.; Reyes, P. Silica supported rhodium metal nanoparticles stabilized with (-)-DIOP. Effect of ligand concentration and metal loading on enantioselective hydrogenation of ketones. *J. Chil. Chem. Soc.* **2012**, *57*, 1394–1399. [[CrossRef](#)]
28. Gonzalez-Galvez, D.; Nolis, P.; Philippot, K.; Chaudret, B.; van Leeuwen, P.W.N.M. Phosphine-Stabilized Ruthenium Nanoparticles: The Effect of the Nature of the Ligand in Catalysis. *ACS Catal.* **2012**, *2*, 317–321. [[CrossRef](#)]
29. Tamura, M.; Fujihara, H. Chiral Bisphosphine BINAP-Stabilized Gold and Palladium Nanoparticles with Small Size and Their Palladium Nanoparticle-Catalyzed Asymmetric Reaction. *J. Am. Chem. Soc.* **2003**, *125*, 15742–15743. [[CrossRef](#)] [[PubMed](#)]
30. Sawai, K.; Tatumi, R.; Nakahodo, T.; Fujihara, H. Asymmetric Suzuki–Miyaura Coupling Reactions Catalyzed by Chiral Palladium Nanoparticles at Room Temperature. *Angew. Chem. Int. Ed.* **2008**, *47*, 6917–6919. [[CrossRef](#)] [[PubMed](#)]

31. Cano, I.; Tschan, M.J.-L.; Martínez-Prieto, L.M.; Philippot, K.; Chaudret, B.; van Leeuwen, P.W.N.M. Enantioselective hydrogenation of ketones by iridium nanoparticles ligated with chiral secondary phosphine oxides. *Catal. Sci. Technol.* **2016**, *6*, 3758–3766. [CrossRef]
32. Kamer, P.C.J.; van Leeuwen, P.W.N.M. *Phosphorous (III) Ligands in Homogeneous Catalysis: Design and Synthesis*; Wiley & Sons Inc.: Chichester, UK, 2012; p. 566.
33. Grabulosa, A. *P-Stereogenic Ligands in Enantioselective Catalysis*; RSC Catalysis Series No. 7; Spivey, J.J., Ed.; RSC: Cambridge, UK, 2010; p. 520.
34. Börner, A. *Phosphorus Ligands in Asymmetric Catalysis: Synthesis and Applications*; WILEY-VCH Verlag GmbH & Co. KGaA: Weinheim, Germany, 2008; Volumes 1–3, p. 1546.
35. Aznar, R.; Muller, G.; Sainz, D.; Font-Bardia, M.; Solans, X. Synthesis and Reactivity of P-Chiral Tethered (η^1 : η^6 -phosphinoarene)ruthenium Complexes. *Organometallics* **2008**, *27*, 1967–1969. [CrossRef]
36. Johansson, M.J.; Schwartz, L.; Amedjkouh, M.; Kann, N. New chiral amine ligands in the desymmetrization of prochiral phosphine boranes. *Tetrahedron Asymmetry* **2004**, *15*, 3531–3538. [CrossRef]
37. Lara, P.; Philippot, K.; Chaudret, B. Organometallic Ruthenium Nanoparticles: A Comparative Study of the Influence of the Stabilizer on their Characteristics and Reactivity. *ChemCatChem* **2013**, *5*, 28–45. [CrossRef]
38. Philippot, K.; Chaudret, B. Organometallic approach to the synthesis and surface reactivity of noble metal nanoparticles. *C. R. Chim.* **2003**, *6*, 1019–1034. [CrossRef]
39. Favier, I.; Gómez, M.; Teuma, E. Palladium and ruthenium nanoparticles: Reactivity and coordination at the metallic surface. *C. R. Chim.* **2009**, *12*, 533–545. [CrossRef]
40. López-Vinasco, A.M.; Favier, I.; Pradel, C.; Huerta, L.; Guerrero-Ríos, I.; Teuma, E.; Gómez, M.; Martin, E. Unexpected bond activations promoted by palladium nanoparticles. *Dalton Trans.* **2014**, *43*, 9038–9044. [CrossRef] [PubMed]
41. Favier, I.; Massou, S.; Teuma, E.; Philippot, K.; Chaudret, B.; Gómez, M. A new and specific mode of stabilization of metallic nanoparticles. *Chem. Commun.* **2008**, 3296–3298. [CrossRef] [PubMed]
42. Favier, I.; Lavedan, P.; Massou, S.; Teuma, E.; Philippot, K.; Chaudret, B.; Gómez, M. Hydrogenation Processes at the Surface of Ruthenium Nanoparticles: A NMR Study. *Top. Catal.* **2013**, *56*, 1253–1261. [CrossRef]
43. Chahdoura, F.; Pradel, C.; Gómez, M. Palladium Nanoparticles in Glycerol: A Versatile Catalytic System for C-X Bond Formation and Hydrogenation Processes. *Adv. Synth. Catal.* **2013**, *355*, 3648–3660. [CrossRef]
44. Tschan, M.J.-L.; Diebolt, O.; van Leeuwen, P.W.N.M. Ruthenium Metal Nanoparticles in Hydrogenation: Influence of Phosphorus-Ligands. *Top. Catal.* **2014**, *57*, 1054–1065. [CrossRef]
45. Escárcega-Bobadilla, M.V.; Tortosa, C.; Teuma, E.; Pradel, C.; Orejón, A.; Gómez, M.; Masdeu-Bultó, A.M. Ruthenium and rhodium nanoparticles as catalytic precursors in supercritical carbon dioxide. *Catal. Today* **2009**, *148*, 398–404. [CrossRef]
46. Rafter, E.; Gutmann, T.; Löw, F.; Buntkowsky, G.; Philippot, K.; Chaudret, B.; van Leeuwen, P.W.N.M. Secondary phosphine oxides as pre-ligands for nanoparticle stabilization. *Catal. Sci. Technol.* **2013**, *3*, 595–599. [CrossRef]
47. Jiang, H.-Y.; Zhen, X.-X. Tuning the chemoselective hydrogenation of aromatic ketones, aromatic aldehydes and quinolines catalyzed by phosphine functionalized ionic liquid stabilized ruthenium nanoparticles. *Catal. Sci. Technol.* **2015**, *5*, 3728–3734. [CrossRef]
48. Wu, Z.; Jiang, H. Efficient palladium and ruthenium nanocatalysts stabilized by phosphine functionalized ionic liquid for selective hydrogenation. *RSC Adv.* **2015**, *5*, 34622–34629. [CrossRef]
49. Delbecq, F.; Loffreda, D.; Sautet, P. Heterogeneous Catalytic Hydrogenation: Is Double Bond/Surface Coordination Necessary? *J. Phys. Chem. Lett.* **2010**, *1*, 323–326. [CrossRef]
50. Bera, T.; Thybaut, J.W.; Marin, G.B. Extension of the Single-Event Microkinetic Model to Alkyl Substituted Monoaromatics Hydrogenation on a Pt Catalyst. *ACS Catal.* **2012**, *2*, 1305–1318. [CrossRef]

